Optical Setup for a Piston-Cylinder Pressure Cell: A Two-Volume Approach

Pavel Naumov,[1] Ritu Gupta,[2] Marek Bartkowiak,[3] Ekaterina Pomjakushina,[4] Nicola P.M. Casati,[5] Matthias Elender,[2,*] and Rustem Khasanov[2,†]

[1] *Quantum Criticality and Dynamics Group, Paul Scherrer Institut, Villigen PSI CH-5232, Switzerland*
[2] *Laboratory for Muon Spin Spectroscopy, Paul Scherrer Institute, Villigen PSI CH-5232, Switzerland*
[3] *Laboratory for Neutron and Muon Instrumentation, Paul Scherrer Institute, Villigen PSI CH-5232, Switzerland*
[4] *Laboratory for Multiscale Materials Experiments, Paul Scherrer Institut, Villigen PSI CH-5232, Switzerland*
[5] *Laboratory for Synchrotron Radiation – Condensed Matter, Paul Scherrer Institut, Villigen PSI CH-5232, Switzerland*

(Received 15 November 2021; revised 4 January 2022; accepted 26 January 2022; published 24 February 2022)

Measurement of the absolute value of the applied pressure in high-pressure muon and neutron experiments is a complicated task. It often requires the presence of a calibration material inside the sample volume, and could also cause additional time to obtain the response of the calibrant. Here we describe the use of optical calibrants for precise determination of the pressure value inside the piston-cylinder clamp cells. Utilizing the concept of separate volumes for the sample and the optical media, a setup for conducting *in situ* pressure measurements is successfully tested. Pressures in both the "sample" and the "optical" volumes are proved to be the same within experimental accuracy. The use of $SrB_4O_7 : (0.01\ Sm^{2+}, 0.03\ Eu^{2+})$ as a pressure calibrant allows for a high accuracy of pressure determination by considering up to eight fluorescence lines.

DOI: 10.1103/PhysRevApplied.17.024065

I. INTRODUCTION

Experiments under high pressure represent an integral field in condensed-matter physics. Currently, large neutron and muon research user facilities are equipped with various types of high-pressure devices allowing for experiments in high magnetic fields (up to several tens of tesla) and low temperatures (down to few millikelvin). Among the many different types of cells, one of the most popular remains the clamp-type construction, which allows one to reach pressures as high as $p \simeq 3$ GPa and is characterized by a reasonably large volume of the sample chamber compared to its compact pressure-cell dimensions [1,2].

Measurement of the absolute value of the pressure inside the piston-cylinder clamp cells used in neutron and muon-spin rotation and relaxation (μSR) experiments is a complicated task. Generally, the sample is loaded, pressurized, and locked at room temperature outside of the neutron and muon beam. Pressure determination in clamp cells are separated, therefore, in "*ex situ*" and "*in situ*" measurements.

For "*ex situ*" measurements, the pressure is determined outside of the neutron and muon spectrometer. There are two possible ways to make the pressure determination: (i) the "contact" or (ii) the "contactless" methods are generally considered. In case (i), the connection (contact) wires enter the cell [1,2]. The pressure is typically determined by measuring resistivity of a manganin wire, or the superconducting transition of some elemental metals, such as Sn, In, or Pb [1–4]. The disadvantage of the "contact"-type of pressure determination is that one needs to introduce the current leads inside the volume of the cell, where the high pressure is generated. Therefore, special attention must be given in the preparation of the feedthrough, which must allow the current leads to enter, but also must be strong enough to not be blown out by the pressure generated inside the cell [1,5]. In case (ii), i.e., in the "contactless" case, the pressure is determined by measuring the ac response of elemental superconductors as Sn, In, or Pb [6,7], the optical response of the fluorescence material [8], or the enhancement of the pressure-cell outer diameter [7]. The disadvantage of a "contactless" case is that one needs either to find a way to access the pressure probe (optical or superconducting) via the clamped cell body or calibrate the enhancement of the cell diameter as a function of pressure inside the cell.

The "*in situ*" pressure determination in neutron experiments is typically performed by measuring the unit-cell parameters of a material with a known equation of state (such as NaCl, MgO, or Pb) mixed with the sample [2,9]. This method has several disadvantages, since the calibrant

*matthias.elender@psi.ch
†rustem.khasanov@psi.ch

 © 2022 American Physical Society

material reduces much needed sample volume, may absorb neutrons, or could even react with the sample. In μSR studies the "*in situ*" pressure determination is possible only in three experiments, where the sample itself (Al, In, and Sr_2RuO_4, Refs. [10–12]) is used as the pressure calibrant.

It is thus crucial to monitor the pressure inside the cell without reducing the volume available for the sample. It could also be useful, for some experiments, to prevent a mixing of the sample and the pressure indicator materials. For resolving the above issues, the concept of a double-volume pressure cell, where the "optical" and the "sample" volumes are physically separated from each other, is developed and successfully tested. The construction of the piston-cylinder cell is modified by introducing the tungsten carbide piston with the entrance for the optical fibers, the teflon seal with the conical cavity, and the optical window made of commercially available cubic-zirconia single crystals.

The paper is organized as follows: Sec. II describes the concept of a double-volume piston-cylinder clamp cell and the optical setup for pressure determination. The description of the double-volume pressure-cell assembly is given in Sec. III. The parts of the optical setup, the optical window and the teflon mushroom, are discussed in Secs. III A and III B, respectively. The results of calibration of the optical sensor, SrB_4O_7 : $(0.01\ Sm^{2+}, 0.03\ Eu^{2+})$, are presented in Sec. IV. Section V describes the test results of the double-volume pressure cell. The finite-element analysis data are described in Sec. VI. Conclusions follow in Sec. VII.

II. THE CONCEPT OF THE DOUBLE-VOLUME CLAMP CELL AND MEASURING PRINCIPLE

The "double-volume" concept accounts for the physical separation of the two volumes (the first occupied by the sample and the second by the pressure probe). An example of such a design is presented at the top left corner of Fig. 1, where the large yellow oval and the small yellow circle represent the sample and the pressure probe volume, respectively. The crucial condition of such a design is that the partitioning material transmits the pressure perfectly.

The double-volume clamp cell may expect to have several advantages since the following holds.

(i) The calibrant material does not mix with the sample, so any possible reaction between the sample and the calibrant is not possible.

(ii) The optical probe stays away from the sample region and will thus not be hit by neutrons or muons with properly collimated beams.

(iii) The volume occupied by the optical probe is far smaller compared to the sample volume. Indeed, the fluorescence measurements could be easily performed on a small ruby crystal (approximately 0.01 mm^3 or less), while the "sample" volume for a typical piston-cylinder clamp cell used in neutron and muon experiments is of the order of 200–500 mm^3 [6–8,11,16–18].

(iv) Both the "sample" and the "optical" volumes could be connected via a channel drilled inside the pressure seal (thin dashed lines in Fig. 1 marked as "possible connection between volumes").

The measurement setup, as is shown in Fig. 1, includes the laser source, the optical spectrometer, the optical reflection probe, and the controlling PC. In our experiments, the excitation light is provided by a 520-nm PLM-520.0-MMF-0.1 Solid-State Laser from "Lasercomponents" with a maximum power of 25 mW [13]. The fluorescence spectra are measured using HR4000 or HR4PRO spectrometers from "Ocean Optics" [14]. The optical reflection probe with the 1.4 mm ferrule terminated fibers is obtained from the Art Photonics [15]. The control PC has the "OceanView" and laser operation software installed [13,14].

III. THE DOUBLE-VOLUME PRESSURE-CELL ASSEMBLY

A schematic view of a double-volume clamp cell is presented in Fig. 2(a). The pressure-cell body (with the inner and the outer diameters ∅6 and ∅24 mm, respectively) and the top part of the pressure seal [the mushroom, the tungsten carbide (WC) piston, the WC pressing pad, and the fixation bolt] are the same as currently used in clamped cells for muon-spin rotation and relaxation experiments [6,7,11], and are not discussed here.

The expanded view of the "optical" part is presented in Fig. 2(b). It consists of the ∅12 mm WC support disk with a 2-mm hole, the ∅6-mm WC piston with a 1.5-mm hole, the optical window made out of a 4 mm single-crystal piece of cubic-zirconia, and the teflon mushroom with the conical entrance for the optical window. The optical probe ($\simeq 0.1 - 0.5$ mm^3 crystal of ruby and/or a small amount of SrB_4O_7 powder), is placed on the top of the optical window together with a small drop of the pressure transmitting media (Daphne 7373 oil, in our case).

Here below the main elements of the double-volume optical setup, namely the optical window and the teflon mushroom, are described separately.

A. Optical window

The optical window is used to transfer excitation light and collect the reflected light, which contains the fluorescence response of the optical probe (see Fig. 1). This means that the window needs to both be transparent to light and also strong enough to withstand high pressure. In the vast majority of pressure experiments, the media used for optical windows are either sintered diamond or sapphire [1,2,8,19,20]. Recently, cubic-zirconia (c-zirconia)

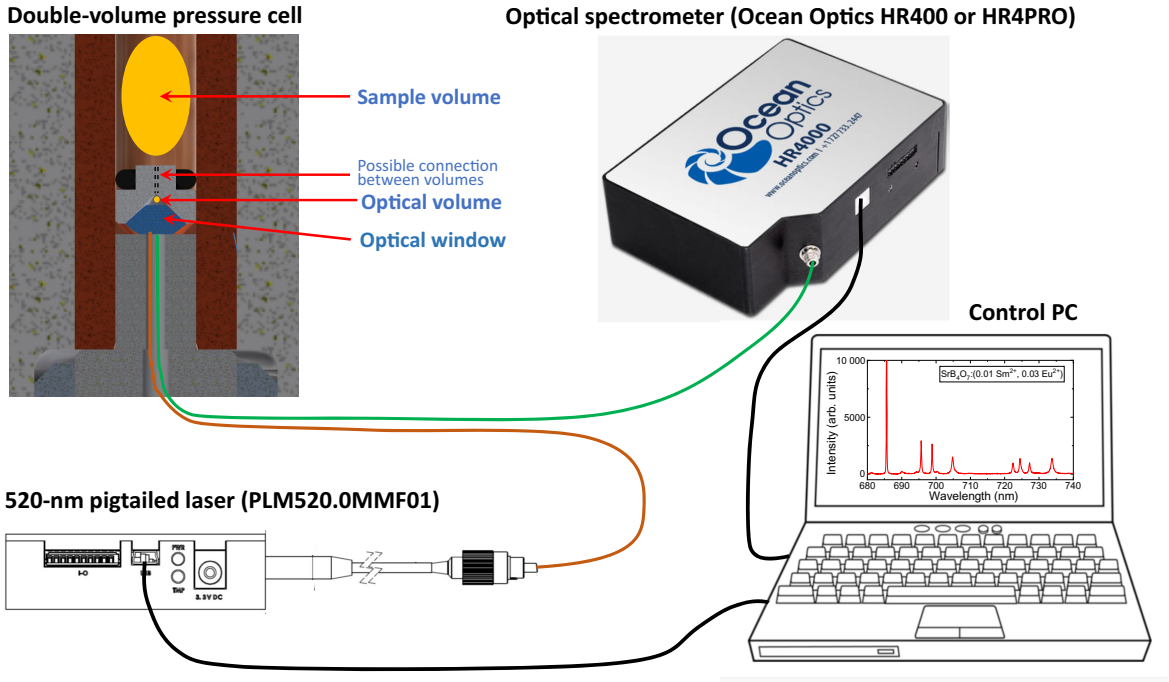

FIG. 1. The concept and the pressure measuring principle of the double-volume clamp cell. The pressure cell (top left corner) has two separate volumes: the first for the sample (large yellow oval) and the second for the optical probe (small yellow circle). The volumes may be connected via a channel. The measurement setup includes the laser source (PLM-520.0-MMF-0.1 Solid-State Laser from "Lasercomponents", Ref. [13]), the optical spectrometer (HR4000 or HR4PRO from "Ocean Optics", Ref. [14]) and the control PC (with the "OceanView", Ref. [14], and the laser operation, Ref. [13], software). The pressure cell, the excitation laser, and the measuring spectrometer are connected with each other via the optical reflection probe (Art Photonics, Ref. [15]).

and moissanite single crystals have become easily available. They are machined in a so-called "brilliant-cut" shape and are often used in the jewelry industry as a low-cost substitute for diamonds.

Comparison of mechanical properties of different gem stones used in high-pressure experiments are presented in Table I. Here, the "Highest p" row refers to the maximum pressure each material can withstand when used as an anvil in anvil-type pressure cells. Following the results presented in Table I, even cubic-zirconia is suitable for use as an optical window in clamp-type cells, where maximum pressures typically do not exceed $\simeq 3$ GPa. Cubic-zirconia is therefore chosen as the primary material for the developments presented in this paper.

TABLE I. Comparison of mechanical properties of different gem stones, after Refs. [21,22]. The prices are taken from Refs. [19,23]. The row "Highest p" refers to the maximum pressure for the materials used as an anvil in anvil-type pressure cells.

	Diamond	Moissanite	Sapphire	c-zirconia
Composition	C	SiC	Al_2O_3	ZrO_2
Hardness (Mohr)	10	9.25	9	8.5
Highest p (GPa)	640	58.7	25.8	16.7
Price (USD)	800–1200	10	20	0.2

Figure 3(a) shows schematically the commercially available gem stone in the so-called "brilliant-cut" shape. The sharp and the flat parts of the crystal are called the "culet" and the "table," respectively. The "table" is utilized as a light entrance window. One of the features of the "brilliant-cut" shape is that the incident light is fully reflected inside the crystal [see Fig. 3(b)]. In our experiments, however, the light should be able to leave the crystal at the culet side, so the "culet" end of the crystal must be flattened [truncated, see Fig. 3(c)].

On the table side, however, the crystals must be truncated for a slightly different motivation. The crystals, used in our optical setup, have a size of 4 mm. As delivered, the average table diameter is $\simeq 2.2$ mm, which is only marginally larger than the 1.5-mm hole in the piston. One clearly needs to increase the contact area between the flat part of the crystal and the piston surface [see Fig. 3(c)].

Figure 4 shows the piston surface when the "table" part of the 4 mm crystal is not cut [Figs. 4(a) and 4(b)] and when it is cut by 0.25 mm [Fig. 4(c)]. Obviously, in the case of a bare crystal, even a single load with the maximum applied force $F_{ap} \simeq 72$ kN (which corresponds to the applied pressure $p_{ap} = F_{ap}/S \simeq 2.5$ GPa, S is the piston's top area) leads to the appearance of an indentation on the surface of the WC piston [Fig. 4(a)], while the repetitive load leads to damage to the piston around the central hole

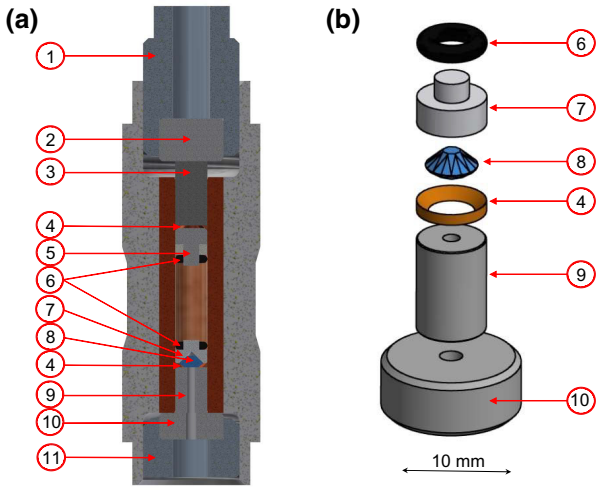

FIG. 2. (a) Cross section view of the double-volume piston-cylinder pressure cell. The pressure-cell body, with the inner and the outer diameters ∅6 and ∅24 mm, respectively, is the same as described in Refs. [6,7,11]. (b) The expanded part of the optical setup. The meaning of the elements are as follows: (1) the top fixation bolt; (2) the top WC pressing pad; (3) the top WC piston; (4) beryllium copper (BeCu) sealing ring; (5) BeCu mushroom; (6) O-ring; (7) teflon mushroom with the conical entrance for the optical window; (8) optical window (c-zirconia crystal); (9) WC piston with a 1.5 mm hole; (10) WC support disk with a 2 mm hole; and (11) the bottom fixation bolt.

[Fig. 4(b)]. The use of the similar crystal, but truncated by $\simeq 0.25$ mm on the table side, increases the contact area between the piston and the crystal and leads to an almost complete disappearance of an indentation step [Fig. 4(c)].

B. Teflon mushroom

The teflon mushroom with the conical entrance for the optical window (Fig. 2), plays a dual role:

(i) The top part of the mushroom's conical entrance works as a pressure volume for the optical probe (see Fig. 1).

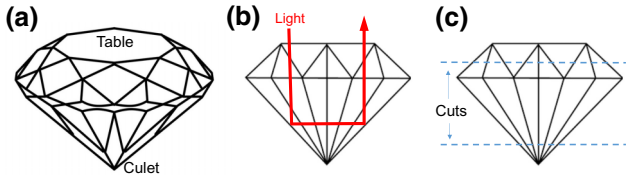

FIG. 3. (a) Schematic representation of a commercial gem stone in the "brilliant-cut" shape. (b) The optical path inside the gem stone. In order to allow the shining light to pass through the crystal, the culet must be flattened. (c) The preparation of the optical window, which requires the crystal truncation on both the table and culet sides.

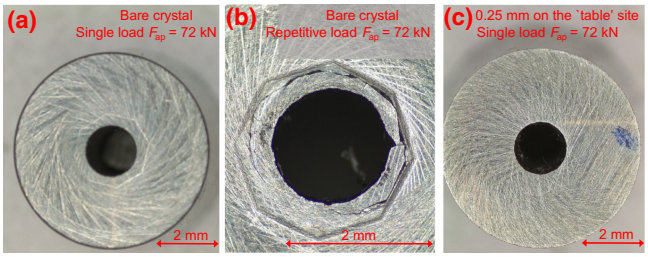

FIG. 4. (a) The top surface of WC piston after applying the force $F_{ap} \simeq 72$ kN to the bare (not truncated) cubic-zirconia crystal. The stamp around the center hole corresponds to the dimension of the crystal's "table." (b) The top surface of WC piston after applying the repetitive load of $F_{ap} \simeq 72$ kN to the bare cubic-zirconia crystal. (c) The same as in (a) but for the crystal with the 0.25 mm truncated "table" part.

(ii) The teflon mushroom seals pressures in both, the sample and optical, volumes.

The pressure in the sample space is sealed as described in Ref. [7]. The initial pressure seal, up to $p \simeq 0.6 - 0.9$ GPa, is made by the rubber O-ring. With the pressure increase, the teflon mushroom deforms and it fills the volume between the beryllium copper (BeCu) sealing ring and the top area of the WC piston. The role of the BeCu ring is to prevent the flow of the teflon further down, i.e., to enter the area between the pressure-cell channel and the walls of the WC piston. The seal of the "optical volume" occurs simultaneously with the seal of the sample space. The teflon mushroom, being deformed by the applied pressure, seals also the optical volume, i.e., the small volume on top of the optical window, which is filled with the fluorescing material and the pressure transmitting media.

It is worthwhile to note that, after opening the pressure cell, both the teflon mushroom and the optical window came out stuck together as one piece. There are two possible ways to proceed:

(i) The mushroom and window piece could be disintegrated (opened) and the assembly of a "new" mushroom with an "old" optical window might be used in the next experiment.

(ii) The mushroom and window assembly remains unopened and is used in the next experiment.

The advantage of (ii) is that there is no need to reload the "optical" volume. Experiments reveal that the mushroom and window assembly might be reused by approximately 3–4 times.

IV. SrB_4O_7 : ($0.01Sm^{2+}$, $0.03Eu^{2+}$) OPTICAL PRESSURE SENSOR

The fluorescence method is widely used for *in situ* pressure determination [1,2]. For measurements in anvil

cells, a small amount of the fluorescence-emitting material (ruby, SrB_4O_7, etc.) is, typically, placed inside the cell together with the sample. In the clamp-type cells, one either enters with the fiber(s) inside the main sample volume [24], or places the optical calibrant between the piston and the teflon cup containing the sample [8].

In the present study, we follow the method outlined by Podlesnyak *et al.* [8], who suggested to use the samarium-doped strontium tetraborate ($SrB_4O_7 : Sm^{2+}$) as a fluorescence sensor for clamp-type pressure cells. In accordance with the literature [8,25,26], $SrB_4O_7 : Sm^{2+}$ has several advantages compared to ruby (the most commonly used optical sensor). In particular, the main excited line, $^7D_0 - {}^5F_0$, has a weak temperature dependence $d\lambda/dT \simeq -10^{-4}$ nm/K compared to $d\lambda/dT \simeq 6.8 \times 10^{-3}$ nm/K for the ruby excitation [8,25–27]. Moreover, the position of the narrow and well-isolated $^7D_0 - {}^5F_0$ Sm^{2+} line could be determined more accurately than the strongly overlapping R1 and R2 peaks in the case of ruby. In addition, in Ref. [28] it was demonstrated that incorporating Eu^{2+} into the crystal structure of $SrB_4O_7 : Sm^{2+}$ may lead to an enhancement ($\simeq 60$ times) of the Sm^{2+} emission.

$SrB_4O_7 : (0.01\ Sm^{2+}, 0.03\ Eu^{2+})$ is prepared in the way described in Ref. [28]. The calibration of $SrB_4O_7 : (0.01\ Sm^{2+}, 0.03\ Eu^{2+})$ is performed in a diamond anvil cell by covering a pressure range from 0 to $\simeq 4.2$ GPa. In this experiment a small ruby chip is placed inside the cell together with SrB_4O_7. The pressure is determined by measuring the pressure-induced shift of the R1 ruby line: $d\lambda_{R1}/dp = 0.365(5)$ nm/GPa [25,29].

Figure 5(a) shows two fluorescence spectra collected in a diamond anvil cell at ambient pressure (black line) and at $p = 4.23$ GPa (red line). Two ruby and eight SrB_4O_7 fluorescence lines are denoted by "R" and "λ" letters, respectively. With increasing pressure, all lines shift to the higher wavelengths. The comparison of the pressure-induced shift of λ_1 and λ_8 fluorescence lines of SrB_4O_7 with the R1 and R2 lines of ruby is presented in Fig. 5(b). It is interesting to note that the pressure shift of λ_8 line, $d\lambda_8/dp = 0.488(7)$ nm/GPa, exceeds the corresponding pressure coefficient of the R1 line of ruby, $d\lambda_{R1}/dp = 0.365(5)$ nm/GPa, by more than 30%.

The results of linear fits to the pressure dependencies of the $SrB_4O_7 : (0.01\ Sm^{2+}, 0.03\ Eu^{2+})$ fluorescence lines are summarized in Table II. For comparison, the data for $SrB_4O_7 : (0.05\ Sm^{2+})$ from Ref. [26] are also included. Obviously, the line positions at ambient pressure and the linear coefficients determined in this work are slightly different from those obtained by Lacam *et al.* in Ref. [26]. Note also, that $d\lambda_1/dp = 0.241$ nm/GPa was reported by Podlesnyak *et al.* in Ref. [8]. The clear difference between our data and that mentioned in the literature imply that the SrB_4O_7-based optical probes are not universal. One needs, therefore, to perform individual calibrations for each newly synthesized SrB_4O_7 batch.

TABLE II. Wavelengths of eight fluorescence lines of $SrB_4O_7 : (0.01\ Sm^{2+}, 0.03\ Eu^{2+})$ at ambient pressure, $\lambda_i(p = 0)$, $i = 1, ..8$, and the corresponding pressure-induced shifts, $d\lambda_i/dp$. The errors are obtained from the linear fits to $\lambda_i(p)$ data [see Fig. 5(b)]. The fourth and the fifth columns show the similar data for $SrB_4O_7 : (0.05\ Sm^{2+})$ from Ref. [26].

Line	$SrB_4O_7 : (0.01\ Sm^{2+}, 0.03\ Eu^{2+})$		$SrB_4O_7 : 0.05\ Sm^{2+}$	
	$\lambda_i(p = 0)$ nm	$d\lambda_i/dp$ nm/GPa	$\lambda_i(p = 0)$ nm	$d\lambda_i/dp$ nm/GPa
λ_1	685.359(6)	0.276(3)	685.41	0.255
λ_2	695.416(9)	0.244(5)	695.53	0.230
λ_3	698.604(9)	0.360(5)	698.67	0.295
λ_4	704.62(1)	0.279(4)	704.66	0.250
λ_5	722.151(5)	0.336(3)	722.24	0.325
λ_6	724.234(4)	0.251(3)	724.29	0.215
λ_7	726.971(9)	0.292(6)	727.05	0.255
λ_8	733.47(1)	0.488(7)	733.64	0.450

V. TEST EXPERIMENTS

A. Pressures inside the "sample" and the "optical" volumes

In order to use the double-volume clamp cell in real experiments, one needs to ensure that pressures inside the "sample" and the "optical" volumes are equal. The relevance of such confirmation becomes obvious by taking into account the details of the pressure application process. The force applied by the external press (F_{ap}) is transferred through the top WC piston and the top mushroom seal to the sample volume and then, via the teflon mushroom, to the optical volume (see Fig. 2). The pressure seal can lead to a large amount of friction [5], so the real pressure inside the cell becomes smaller compared to the applied one ($p < p_{ap}$; $p_{ap} = F_{ap}/S$, S is the piston's top area) during the cell pressurization process, and it is higher than p_{ap} ($p > p_{ap}$) during the cell depressurization procedure [11].

The setup of our test experiments is shown schematically in Fig. 6(a). A standard μSR double-wall piston-cylinder pressure cell [similar to the one shown in Fig. 2(a) and described in Refs. [6,7]] is used. Two pressure indicators (small pieces of elemental metals, Sn and In) are placed inside of the "optical" and the "sample" volumes. Another two "reference" probes are attached to the pressure-cell body. The piston with the optical entrance (1.5 mm central hole) is replaced by the bare one (without hole) and the optical window is not used. The pressure is determined by measuring shifts of the superconducting transition temperatures (T_c's) of In and Sn from their ambient pressure values, $T_c^{In}(p = 0) \simeq 3.405$ K and $T_c^{Sn}(p = 0) \simeq 3.717$ K, by means of the ac susceptibility (ACS) technique. The design and operation of the ACS measuring setup used in our study is described in detail in Ref. [7].

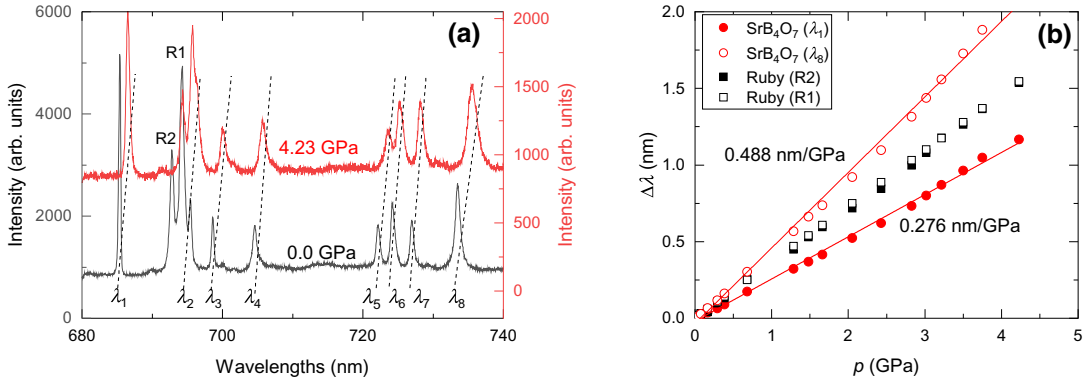

FIG. 5. (a) The fluorescence spectra of ruby and $SrB_4O_7 : (0.01\ Sm^{2+}, 0.03\ Eu^{2+})$ collected at room temperature in diamond anvil cell at ambient pressure (black curve) and at $p = 4.23$ GPa (red curve). The fluorescence spectra of ruby consists of two lines (R1 and R2). The fluorescence spectra of $SrB_4O_7 : (0.01\ Sm^{2+}, 0.03\ Eu^{2+})$ consists of eight lines (from λ_1 to λ_8). The dashed lines represent the pressure-induced shifts of fluorescence lines. (b) Pressure shifts of λ_1 and λ_8 lines of SrB_4O_7 and R1 and R2 lines of ruby. The solid lines are linear fits to $\lambda_1(p)$ and $\lambda_8(p)$ data (see text for details).

Figure 6(b) gives an example of ACS measurements at $p_{ap} \simeq 2.2$ GPa applied at a room temperature. The superconducting transitions of all four pressure indicators are clearly visible and are well separated from each other. For pressure determination the following equations are used [4]:

$$T_c^{In}(p) = T_c^{In}(0) - 0.3812\,p + 0.0122\,p^2 \qquad (1)$$

and

$$T_c^{Sn}(p) = T_c^{Sn}(0) - 0.4823\,p + 0.0207\,p^2. \qquad (2)$$

Here, $T_c(0)$ is the superconducting transition temperature at $p = 0$. In Fig. 6(b), e.g., $T_c^{In}(0)$ and $T_c^{Sn}(0)$ might be

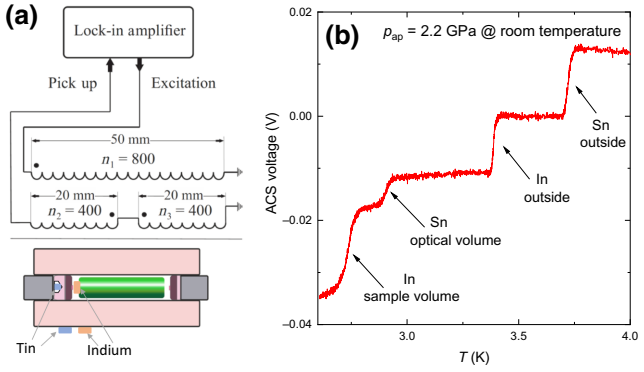

FIG. 6. (a) The ac susceptibility setup used to simultaneous pressure measurements inside the "sample" and the "optical" volumes. The ACS system with the lock-in amplifier and coils (one excitation and two pick up) is the same as described in Ref. [6]. The pressure probes (pieces of Sn and In) are placed inside the "sample" and the "optical" volumes, as well as attached to the pressure-cell body. (b) The ACS curve measured after closing the cell at $p_{ap} \simeq 2.2$ GPa. Arrows mark the superconducting transitions of four pressure probes.

obtained from the transitions marked as "In outside" and "Sn outside," respectively. $T_c^{In}(p)$ and $T_c^{Sn}(p)$ correspond to the superconducting transitions of In and Sn pressure probes mounted into the "sample" and the "optical" volumes, respectively.

The dependence of the pressure inside the "optical" volume as a function of the pressure inside the "sample" volume is presented in Fig. 7(a). The resulting pressures are approached in two different ways: from the lower (black points) and from the higher (red points) pressure values. The corresponding pressure-cell loading curves, representing the displacement of the "top WC piston," Fig. 2(a), as a function of the applied pressure, are shown in Figs. 7(b) and 7(c).

The results presented in Fig. 7 indicate how the double-volume concept, as discussed in Sec. II, works remarkably well. Indeed, pressures inside the "sample" and the "optical" volumes are the same within the experimental accuracy. There is no hysteresis if the final pressure reached from the previously set higher or lower values.

B. Experiments with the fluorescence probe

In order to test the optical measurement setup, as is presented in Fig. 1, the In pressure indicator is placed inside the "sample" chamber and a small drop of a mixture of $SrB_4O_7 : (0.01\ Sm^{2+}, 0.03\ Eu^{2+})$ with the Daphne 7373 oil ($\simeq 0.5 - 1.0$ mm^3) is introduced into the "optical" volume. The results of these test experiments are shown in Fig. 8. Pressures inside the "sample" and the "optical" volumes are determined from the T_c shift of indium and the fluorescence lines of SrB_4O_7, respectively. The fluorescence lines of $SrB_4O_7 : (0.01\ Sm^{2+}, 0.03\ Eu^{2+})$ at ambient pressure and at $p \simeq 2.43$ GPa are shown in Fig. 8(b). The pressure-induced shift of all eight fluorescence lines is clearly visible.

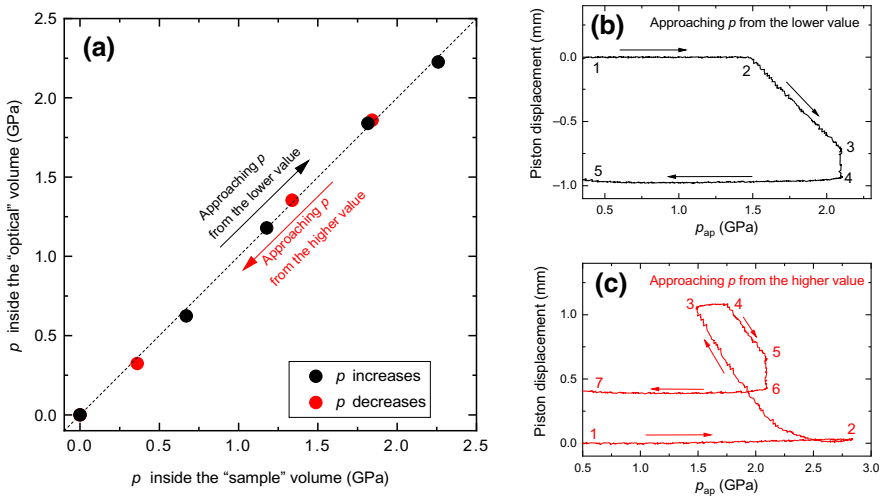

FIG. 7. (a) Dependence of the pressure inside the "optical" volume on the pressure inside the "sample" volume. The dashed line represents the one-to-one correspondence between both pressures. (b) The pressure-cell loading curve representing the process of approaching the final pressure from the lower value. The pressure inside the cell is generated by compressing the pressure transmitting media (Daphne 7373 oil) via applying the external force F_{ap} to the "top WC piston" (Fig. 2). The pressure cell is initially closed (clamped) by tightening the "top fixation bolt" (Fig. 2) at $p_{ap} \simeq 1.5$ GPa. The "top WC piston" is not displaced until p_{ap} reaches a value of 1.5 GPa (the path from point 1 to 2). The piston moves inside the cell with the p_{ap} increase from $\simeq 1.5$ to 2.1 GPa, where the cell is closed by tightening the "top fixation bolt" (the path 2–3–4). The force applied to the bolt leads to an additional movement of the piston by $\simeq 0.2$ mm further down (the path 3–4). By clamping the cell, the position of the piston does not change by releasing p_{ap} down to 0 (path 4–5). (c) The pressure-cell loading curve representing the process of approaching the final pressure from the higher value. The "top fixation bolt" is unscrewed by reaching the point 2. By decreasing p_{ap}, the piston moves outside of the pressure-cell channel (the path 2–3). The rest of the process (the paths 3–4, 4–5, 5–6, and 6–7) is the same as described in (b).

Figure 8(a) shows that the pressure values determined by the use of indium as a pressure indicator are systematically lower ($\simeq 0.2$ GPa) than those obtained by means of SrB_4O_7 fluorescence. Note that the pressure determined via the superconducting transition temperature of In corresponds to the low-temperature value of the pressure ($T \simeq 3$ K), while the fluorescence spectra of SrB_4O_7 are measured at a room temperature. The pressure drop by cooling is typical for piston-cylinder cells and it is caused, mainly, by the thermal contraction of the pressure transmitting media [30]. In our experiments 7373 Daphne oil is used, which is characterized by the pressure drop via cooling of the order of 0.15–0.2 GPa [31,32].

The closed and open symbols in Fig. 8(a) refer to the data taken by using two different cubic-zirconia crystals (no. 1 and no. 2). Crystal 1 is cracked at $p_{ap} \simeq 2.4$ GPa,

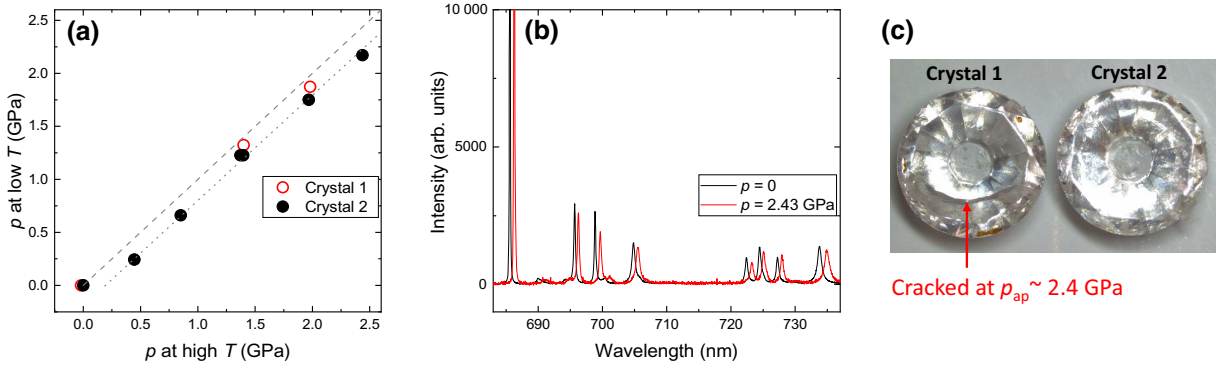

FIG. 8. (a) Dependence of the low-temperature pressure value (at $T \simeq 3$ K, as is determined from the T_c shift of indium) on the high-T pressure (as is obtained in florescence measurements at room temperature). The pressure difference between the high-T and the low-T pressure values is $\simeq 0.2$ GPa, which is typical for piston-cylinder cells and it is caused by the thermal contraction of the pressure transmitting media (Daphne 7373 oil in our case). (b) The fluorescence spectra of SrB_4O_7 : $(0.01\ Sm^{2+}, 0.03\ Eu^{2+})$ at $p = 0$ (black curve) and $p = 2.43$ GPa (red curve). (c) Cubic-zirconia crystals used in this experiment. Crystal 1 is cracked at $p_{ap} \simeq 2.4$ GPa, while crystal 2 survived after several loading cycles with the applied pressure reaching $\simeq 2.8$ GPa.

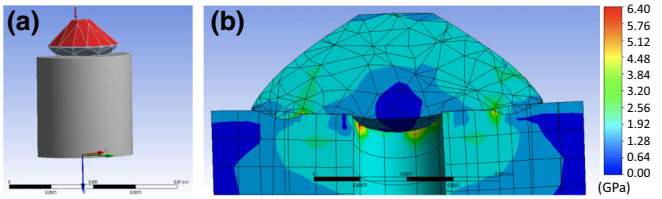

FIG. 9. (a) Finite-element analysis model of the optical window and the WC piston assembly. A pressure of 1 GPa is applied to the top part of the optical window (the red colored area). (b) Distribution of mechanical stresses in the contact area between the top of the WC piston and the optical window.

while crystal 2 survived after several loading cycles with the applied pressure reaching $p_{ap} \simeq 2.8$ GPa. This implies the following:

(i) The maximum pressure of commercially available cubic-zirconia gemstones may vary from crystal to crystal and

(ii) at present conditions, the cubic-zirconia crystals are near their mechanical limit.

VI. FINITE-ELEMENT ANALYSIS

To estimate the amount of mechanical stress on the optical window and the WC piston with 1.5 mm inner hole, the piston and window assembly is modeled using ANSYS finite-element analysis software [33]. The model is set up as shown in Fig. 9(a). The external 1 GPa pressure is applied to the top part of the cubic-zirconia crystal [the red colored area in Fig. 9(a)]. It should be noted here that for simplicity the optical window, i.e., c-zirconia single crystal, is analyzed as an isotropic material. This is a very crude approximation, which allows the study of only the contact surface between the c-zirconia optical window and the WC piston.

The results of the analysis are presented in Fig. 9(b). The maximum load is found in the area around the 1.5 mm hole, i.e., exactly at the place where damages on the WC piston [Fig. 4(b)] and the crack on crystal 1 [Fig. 8(c)] appear. Although the maximum pressure in this area (approximately 6 GPa) is far from the cubic-zirconia pressure limit ($\simeq$ 16.7 GPa, see Table II), the failure of some optical windows may relate to the low quality of commercially available crystals. At the same time, the pressure around the optical entrance exceeds the ultimate tensile stress of the tungsten carbide ($\simeq$ 370 MPa, Ref. [34]) and results in an anvil-shaped indentation of WC piston [see also photos in Figs. 4(a) and 4(b)].

The results of ANSYS simulations support our experimental findings. They suggest that in order to reach repeatedly pressures above 2 GPa by using the optical setup described above, either the diameter of the hole inside the WC piston must be reduced from 1.5 down to, e.g., 1 mm, or the optical window material must be replaced by a "stronger" sapphire, moissanite, or diamond crystals (see Table I).

VII. CONCLUSIONS AND OUTLOOK

To summarize, a double-volume clamp-cell measurement setup is successfully designed and tested. With the present construction, the pressure inside the "optical" and the "sample" volumes are proved to be the same within the experimental accuracy. The present concept could be used with almost all types of piston-cylinder cells and requires just a minor modification of the pressure sealing part.

The advantages of the presently proposed double-volume setup compared to the usual single volume approach are the following:

1. The pressure calibrant stays in a separate volume and it is not mixed with the sample. This allows one to avoid any possible reaction between the sample and the calibrant material.
2. The optical probe stays a few millimeters below the sample so that is not hit by neutrons or muons with properly collimated beams.
3. The volume occupied by the optical probe is of the order of 0.2–0.5 mm^3, which is 2 orders of magnitude smaller than the volume available for the sample in standard muon and neutron pressure cells.

The use of cubic-zirconia windows, produced from commercially available gemstones, is shown to be a reliable and simple approach. On the other hand, the mechanical failure of some cubic-zirconia crystals at pressures exceeding 2 GPa indicates the diverse quality of commercially available gemstones. Sapphire, moissanite, or diamond crystals, with higher mechanical strength, could be used as a reliable, but, however, more expensive replacement. An alternative solution might be the reduction of the optical entrance into the tungsten carbide piston from currently used 1.5 mm, down to 1.0 mm or even smaller. It might be also helpful to increase the contact area between the piston and the optical window by using truncated ball-shaped crystals instead of crystals shaped in a "brilliant cut."

ACKNOWLEDGMENTS

The work is performed at the Swiss Muon Source (SμS), Paul Scherrer Institute (PSI, Switzerland). The work of R.G. is supported by the Swiss National Science Foundation (SNF Grant No. 200021-175935). R.K. acknowledges the help of Charles Hillis Mielke III for carefully reviewing the manuscript.

[1] M. Eremets, *High Pressure Experimental Methods* (Oxford Science Publications, Oxford, New York, Tokyo, 1996).

[2] S. Klotz, *Techniques in High Pressure Neutron Scattering* (Imprint CRC Press, Pub. Location Boca Raton 2013).

[3] W. Wang, D. A. Sokolov, A. D. Huxley, and K. V. Kamenev, Large volume high-pressure cell for inelastic neutron scattering, Rev. Sci. Instrum. **82**, 0739032011..

[4] A. Eiling and J. S. Schilling, Pressure and temperature dependence of electrical resistivity of Pb and Sn from 1-300 K and 0-10 GPa-use as continuous resistive pressure monitor accurate over wide temperature range; superconductivity under pressure in Pb, Sn and In, J. Phys. F: Met. Phys. **11**, 623 (1981).

[5] I. R. Walker, Nonmagnetic piston–cylinder pressure cell for use at 35 kbar and above, Rev. Sci. Instrum. **70**, 3402 (1999).

[6] R. Khasanov, Z. Guguchia, A. Maisuradze, D. Andreica, M. Elender, A. Raselli, Z. Shermadini, T. Goko, F. Knecht, E. Morenzoni, and A. Amato, High pressure research using muons at the Paul Scherrer Institute, High Press. Res. **36**, 140 (2016).

[7] Z. Shermadini, R. Khasanov, M. Elender, G. Simutis, Z. Guguchia, K. V. Kamenev, and A. Amato, A low-background piston-cylinder type hybrid high pressure cell for muon-spin rotation/relaxation experiments, High Press. Res. **37**, 449 (2017).

[8] A. Podlesnyak, M. Loguillo, G. M. Rucker, B. Haberl, R. Boehler, G. Ehlers, L. L. Daemen, D. Armitage, M. D. Frontzek, and M. Lumsden, Clamp cell with in situ pressure monitoring for low-temperature neutron scattering measurements, High Press. Res. **38**, 482 (2018).

[9] D. L. Decker, High-pressure equation of state for NaCl, KCl, and CsCl, J. Appl. Phys. **42**, 3239 (1971).

[10] R. Khasanov and I. I Mazin, Anomalous gap ratio in anisotropic superconductors: Aluminum under pressure, Phys. Rev. B **103**, L060502 (2021).

[11] R. Khasanov, R. Urquhart, M. Elender, and K. Kamenev, Three-wall piston-cylinder type pressure cell for muon-spin rotation/relaxation experiments, High Pressure Research via Early Access (2021).

[12] R. Khasanov, *et al.*, unpublished.

[13] https://www.lasercomponents.com/de-en/.

[14] https://www.oceaninsight.com/.

[15] https://artphotonics.com/.

[16] R. A. Sadykov, Th. Strassle, A. Podlesnyak, L. Keller, B. Fak, and J. Mesot, High-pressure cells for study of condensed matter by diffraction and inelastic neutron scattering at low temperatures and in strong magnetic fields, J. Phys.: Conf. Ser. **941**, 012082 (2017).

[17] R. Sadykov, C. Pappas, L. J. Bannenberg, R. M. Dalgliesh, P. Falus, C. Goodway, and E. Lelièvre-Berna, 1.5 GPa compact double-wall clamp cell for SANS and NSE studies at low temperatures and high magnetic fields, J. Neutron Res. **20**, 25 (2018).

[18] V. Grinenko, D. Das, R. Gupta, B. Zinkl, N. Kikugawa, Y. Maeno, C. W. Hicks, H.-H. Klauss, M. Sigrist, and R. Khasanov, Unsplit superconducting and time reversal symmetry breaking transitions in Sr_2RuO_4 under hydrostatic pressure and disorder, Nat. Commun. **12**, 3920 (2021).

[19] https://diamondanvils.com.

[20] I. N. Goncharenko, Neutron diffraction experiments in diamond and sapphire anvil cells, High Press. Res. **24**, 193 (2004).

[21] J. Xu, H. Mao, and R. J. Hemley, The gem anvil cell: High-pressure behaviour of diamond and related materials, J. Phys.: Condens. Matter **14**, 11549 (2002).

[22] L. Dubrovinsky, N. Dubrovinskaia, V. Prakapenka, and M. Abakumov, Implementation of micro-ball nanodiamond anvils for high-pressure studies above 6 Mbar, Nat. Commun. **3**, 1163 (2012).

[23] www.aliexpress.com.

[24] K. Koyama-Nakazawa, M. Koeda, M. Hedo, and Y. Uwatoko, In situ pressure calibration for piston cylinder cells via ruby fluorescence with fiber optics, Rev. Sci. Instrum. **78**, 066109 (2007).

[25] F. Datchi, R. LeToullec, and P. Loubeyre, Improved calibration of the $SrB_4O_7 : Sm^2+$ optical pressure gauge: Advantages at very high pressures and high temperatures, J. Appl. Phys. **81**, 3333 (1997).

[26] A. Lacam and C. Chateau, High-pressure measurements at moderate temperatures in a diamond anvil cell with a new optical sensor: $SrB_4O_7 : Sm^2+$, J. Appl. Phys. **66**, 366 (1989).

[27] J. D. Barnett, S. Block, and G. J. Piermarini, An optical fluorescence system for quantitative pressure measurement in the diamond-anvil cell, Rev. Sci. Instrum. **44**, 1 (1973).

[28] T. Zheng, M. Runowski, P. Woźny, S. Lis, and V. Lavín, Huge enhancement of Sm^2+ emission via Eu^2+ energy transfer in a SrB_4O_7 pressure sensor, J. Mater. Chem. C **8**, 4810 (2020).

[29] G. Piermarini, S. Block, J. D. Barnett, and R. Forman, Calibration of the pressure dependence of the R1 ruby fluorescence line to 195 kbar, J. Geophys. Res. Solid Earth **46**, 2774 (1975).

[30] M. S. Torikachvili, S. K. Kim, E. Colombier, S. L. Bud'ko, and P. C. Canfield, Solidification and loss of hydrostaticity in liquid media used for pressure measurements, Rev. Sci. Instrum. **86**, 123904 (2015).

[31] K. Yokogawa, K. Murata, H. Yoshino, and S. Aoyama, Solidification of high-pressure medium Daphne 7373, Jpn. J. Appl. Phys. **46**, 3636 (2007).

[32] D. Stasko, J. Prchal, M. Klicpera, S. Aoki, and M. Murata, Pressure media for high pressure experiments, Daphne oil 7000 series, High Press. Res. **40**, 525 (2020).

[33] https://www.ansys.com/.

[34] https://material-properties.org/tungsten-carbide-properties-application-price/.